



Pluri-decadal (1955–2014) evolution of glacier–rock glacier transitional landforms in the central Andes of Chile (30–33° S)

Sébastien Monnier¹ and Christophe Kinnard²

¹Instituto de Geografía, Pontificia Universidad Católica de Valparaíso, Valparaíso, Chile

²Département des Sciences de l'Environnement, Université du Québec à Trois-Rivières, Trois-Rivières, Québec, Canada

Correspondence to: Sébastien Monnier (sebastien.monnier.ucv@gmail.com)

Received: 7 March 2016 – Discussion started: 22 March 2016

Revised: 5 April 2017 – Accepted: 17 May 2017 – Published: 29 August 2017

Abstract. Three glacier–rock glacier transitional landforms in the central Andes of Chile are investigated over the last decades in order to highlight and question the significance of their landscape and flow dynamics. Historical (1955–2000) aerial photos and contemporary (>2000) Geoeye satellite images were used together with common processing operations, including imagery orthorectification, digital elevation model generation, and image feature tracking. At each site, the rock glacier morphology area, thermokarst area, elevation changes, and horizontal surface displacements were mapped. The evolution of the landforms over the study period is remarkable, with rapid landscape changes, particularly an expansion of rock glacier morphology areas. Elevation changes were heterogeneous, especially in debris-covered glacier areas with large heaving or lowering up to more than $\pm 1 \text{ m yr}^{-1}$. The use of image feature tracking highlighted spatially coherent flow vector patterns over rock glacier areas and, at two of the three sites, their expansion over the studied period; debris-covered glacier areas are characterized by a lack of movement detection and/or chaotic displacement patterns reflecting thermokarst degradation; mean landform displacement speeds ranged between 0.50 and 1.10 m yr^{-1} and exhibited a decreasing trend over the studied period. One important highlight of this study is that, especially in persisting cold conditions, rock glaciers can develop upward at the expense of debris-covered glaciers. Two of the studied landforms initially (prior to the study period) developed from an alternation between glacial advances and rock glacier development phases. The other landform is a small debris-covered glacier having evolved into a rock glacier over the last half-century. Based on these results it is proposed that morphological and dynamical interactions between glaciers and permafrost and their resulting hybrid landscapes may enhance the resilience of the mountain cryosphere against climate change.

1 Introduction

Glacier–rock glacier interactions related to Holocene glacier fluctuations (e.g. Haeberli, 2005) and the current evolution of small debris-covered glaciers having survived to the post-Little Ice Age (LIA) warming (e.g. Bosson and Lambiel, 2016) are important issues in high-mountain studies. They may provide key insights into the mechanisms of rock glacier development (Dusik et al., 2015) and of cryosphere stability and resilience against climate changes; the latter topic

is of societal importance in arid–semiarid mountain areas, where the potential permanence of underground solid water resources subsequent to deglaciation may constitute a non-negligible water resource (e.g. Rangecroft et al., 2013).

The most striking geomorphological expression of glacier–rock glacier interactions is large glacier–rock glacier transitional landforms, which are assemblages of debris-covered glaciers in their upper part and rock glaciers in their lower part (e.g. Käab et al., 1997; Krainer and Mostler, 2000; Ribolini et al., 2007; Monnier et al., 2014; Janke et al., 2015).

Here, it is important to recall and highlight the differences between both types of landforms (Nakawo et al., 2000; Kääb and Weber, 2004; Haeberli et al., 2006; Degenhardt, 2009; Benn and Evans, 2010; Berthling, 2011; Cogley et al., 2011). Rock glaciers are perennially frozen homo- or heterogeneous ice–rock mixtures covered with a continuous and several-metre-thick ice-free debris layer that thaws every summer (known as the permafrost “active layer”); rock glacier movement is governed by gravity-driven permafrost creep. Debris-covered glaciers are glaciers covered with a thin (no more than several decimetres thick) and generally discontinuous debris layer; debris-covered glaciers movement is governed by gravity-driven ice creep and sometimes basal slip in response to a mass balance gradient; debris-covered glaciers do not require permafrost conditions. Rock glaciers and debris-covered glaciers exhibit distinct morphologies that are of critical importance in the surface energy balance and sub-surface heat transfer. On their surface, rock glaciers exhibit “the whole spectrum of forms created by cohesive flows” (Barsch, 1992, p. 176) of “lava-stream-like ... viscous material” (Haeberli, 1985, p. 92). These features vary for each case and study area; according to our field surveys in the Andes, they can be grouped into three main types: small-scale (< 1 m high) ripples or undulations resulting from deformations in the active debris layer moving together with the underlying perennially frozen core, medium-scale (1–5 m high) ridge-and-furrow assemblages resulting from the compression of the whole ice-debris mixture, and large-scale (5–20 m thick and > 100 m long) superimposed flow lobes upon which the first two feature types may naturally appear. Hereafter, we will simply refer to these features as “cohesive flow-evocative features”. Contrarily, debris-covered glaciers are characterized by a chaotic distribution of features evocating surface instability such as hummocks, collapses, crevasses, meandering furrows, and thermokarst depressions and ponds. As a consequence, on rock glaciers the large- and fine-scale surface topography is rather smooth and convex, whereas on debris-covered glaciers it is rather rough and concave. Another morphological difference is the presence of ice visible from the surface: whereas ice is generally invisible from the surface of rock glaciers, it is frequently exposed on debris-covered glaciers due to the discontinuity of the debris cover or the occurrence of the aforementioned morphological features. Finally, and correlatively, over pluri-annual to pluri-decadal periods the morphology of well-developed rock glaciers is quite stable (besides cases of climate warming-related destabilizations, the geometry of surface features evolves but their overall pattern remains the same), while debris-covered glacier morphology is characterized by instability (surface features rapidly appear and disappear).

According to the literature at least three types of glacier–rock glacier interactions can be distinguished:

- i. The readvance(s) and superimposition/embedding of glaciers or debris-covered glaciers onto/into rock glaciers, with related geomorphological and thermal consequences (Lugon et al., 2004; Haeberli, 2005; Kääb and Kneisel, 2006; Ribolini et al., 2007, 2010; Bodin et al., 2010; Monnier et al., 2011, 2014; Dusik et al., 2015). This is the *sensu stricto* significance of “glacier–rock glacier relationships” (Haeberli, 2005) as defined by what has been called the “permafrost school” in reference to the long-term “rock glacier controversy” (see Berthling, 2011).
- ii. The continuous derivation of a rock glacier from a debris-covered glacier by evolution of the surface morphology (see above) together with the conservation and creep of a massive and continuous core of glacier ice (e.g. Potter, 1972; Johnson, 1980; Whalley and Martin, 1992; Potter et al., 1998; Humlum, 2000). This process was not initially called a “glacier–rock glacier relationship”; this view is indeed held by what has been called the “continuum school”, in opposition to the permafrost school (Berthling, 2011). Nevertheless, such a phenomenon does belong, literarily, to the domain of glacier–rock glacier interactions.
- iii. The transformation of a debris-covered glacier into a rock glacier not only by the evolution of the surface morphology but also by the evolution of the inner structure, i.e. the transformation of the debris-covered continuous ice body into a perennially frozen ice–rock mixture by addition from the surface of debris and periglacial ice and fragmenting of the initial glacier ice core. This has been described as an alternative to the dichotomous debate between the permafrost school and continuum school (Monnier and Kinnard, 2015); such phenomenon has been described as achievable over a human-life or historical timescale (Schroder et al., 2000; Monnier and Kinnard, 2015; Seppi et al., 2015).

In the present study, we aim to provide insights into the aforementioned issue using the variety of glacier–rock glacier transitional landforms encountered in the semiarid Andes of Chile and Argentina. These landforms have shown a particularly rapid evolution over the last decades which allow studying glacier–rock glacier interactions on an historical timescale. Three landforms with distinct morphologies have been chosen in the central Andes of Chile in an attempt to diagnose their geomorphological significance, especially in terms of glacier–rock glacier interactions and cryosphere persistence in the current climatic context. To this purpose, this study makes use of aerial and satellite imagery and remote sensing techniques in order to document the morphological and dynamical evolution of the studied landforms over a pluri-decadal time span.

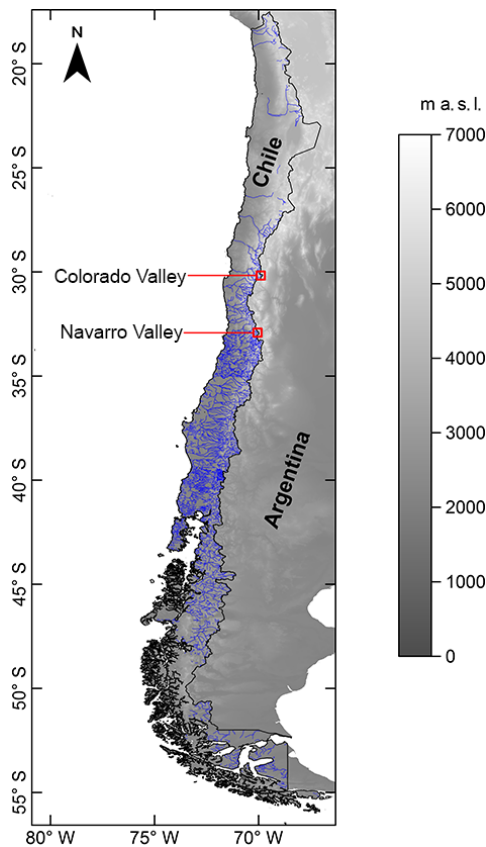


Figure 1. Location of the study sites. Drainage network, which reflects the variations in climatic–hydrologic conditions along the Chilean territory, is shown in blue.

2 Study sites

We studied three glacier–rock glacier transitional landforms in the central Andes of Chile, respectively named Navarro, Presenteseracae, and Las Tetras (Fig. 1). Navarro and Presenteseracae are located in the Navarro Valley, in the upper Aconcagua River catchment (33° S). Las Tetras is located in the Colorado Valley, in the upper Elqui River catchment (30° S).

2.1 Upper Navarro Valley

The upper Navarro Valley belongs to the Juncal River catchment and Juncal Natural Park, which are part of the upper Aconcagua River catchment, in the Valparaíso region of Chile (32°53' S, 70°02' W; Fig. 1). In the Juncal River catchment (~1400–6110 m a.s.l.), glaciers cover 14 % of the area (Bown et al., 2008; Ragettli et al., 2012) while active rock glaciers cover almost 8 % (Monnier and Kinnard, 2015). The climate is a mediterranean mountain climate. Brenning (2005) and Azócar and Brenning (2010) located the 0 °C isotherm of mean annual air temperature (MAAT) close to 3700 m a.s.l. and reported precipitations above

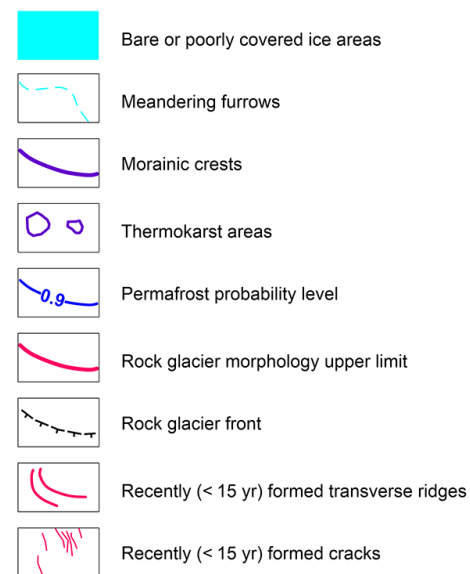


Figure 2. Geomorphological legend shared for all subsequent figures.

3000 m a.s.l. as ranging between 700 and 800 mm yr⁻¹. An automatic weather station located at 2800 m a.s.l. at the foot of the Juncal Glacier, 10 km SW from Navarro Valley, recorded a MAAT of 6.3 °C during the hydrological year 2013–2014. The upper Navarro Valley crosses, from west to east, the Albánico Formation (Upper Cretaceous; andesites, volcanic breccias), the San José Formation (Lower Cretaceous; limestones), and the Lagunilla Formation (Upper Jurassic; sandstones, lutites, gypsum). The glacial footprint is conspicuous through the Navarro Valley: the valley is U-shaped, with corries in the upper parts and latero-frontal moraines in the lower parts (Figs. 2 and 3).

2.1.1 Navarro

Navarro fills the major part of the upper Navarro Valley floor between ~3950 and 3450 m a.s.l. (Fig. 3). The landform was described by Janke et al. (2015, p. 117) as a system composed of several classes of debris-covered glaciers and rock glaciers according to their presumed ice content. It is indeed a huge (>2 km long and up to >1 km wide) and complex assemblage with debris-covered glacier morphology in its upper parts and rock glacier morphology in its lower parts. The main presumed flow direction of the landform points towards 170° N. At least 10 conspicuous and sometimes >15 m high morainic crests are visible at the surface of the landform, some of them being included in the rock glacier morphological unit. At one location (red circle in Fig. 3), the superposition of two series of morainic crests onto a rock glacier lobe suggests that the landform developed from a succession of glacier advances and rock glacier development phases.

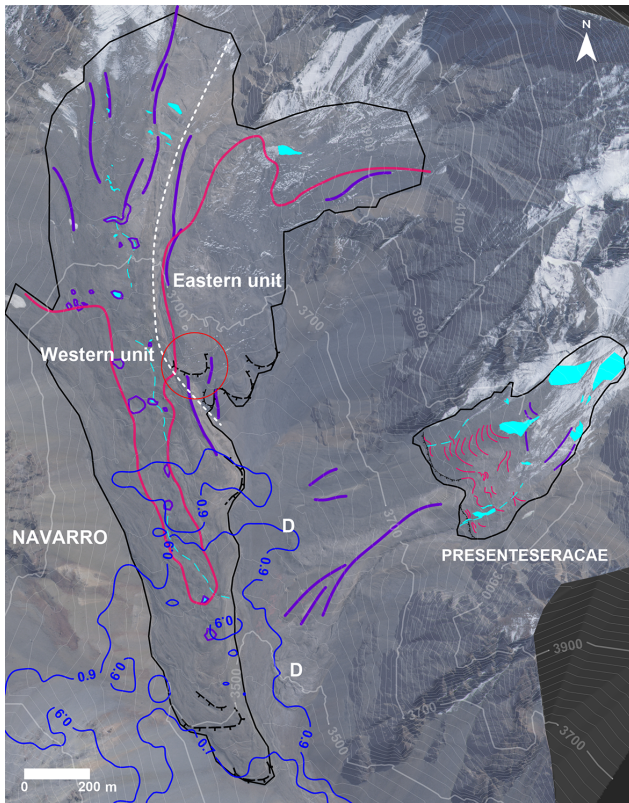


Figure 3. Map of the Navarro Valley. See Fig. 2 for legend. The background of the map is the 2014 Geoeye image draped over the Geoeye DEM (see the “Material and methods” section). Elevation contours are derived from the Geoeye DEM and the contour interval is 20 m. The boundary between the Navarro’s western and eastern units is indicated with a dashed white line. The red circle indicates the location described in the text where morainic crests and rock glacier lobes are superimposed. Note also the decayed (D) rock glacier lobes in the area between Navarro and Presenteseracae.

Navarro is divided between an eastern and a western unit, with the two being separated by a central series of aligned morainic crests (Fig. 3). The eastern unit, which is located in the more shadowed northeastern part of Navarro Valley, is ~ 1.2 km long, and about two-thirds of its area exhibits a rock glacier morphology. The terminal part exhibits three adjacent terminal lobes. The western unit is ~ 2.4 km long and more complex. Sets of embedded morainic crests in the upper part delimit the retreat of a former glacier. The median part (~ 1 km long) is peculiar, with the boundary between the debris-covered and rock glacier morphology extending far downslope and following the contour of an elongated central depression (10–15 m lower in altitude than the lateral margins) (Figs. 3 and 4). This central depression is characterized by numerous large (up to 50 m of diameter) thermokarst depressions with bare ice exposures, generally on their south-facing walls. The lower part of the western unit exhibits a rock glacier morphology and three superim-

posed fronts close to the terminus, the slope of the lowest front being gentler than that of the two upper fronts, which are almost at the same location.

Monnier and Kinnard (2015) provided an empirical model of permafrost probability based on logistical regression for the upper Aconcagua River catchment. According to this model, Navarro may be in a permafrost state. The permafrost probability is close to 1 in the upper parts; nevertheless, there is a marked decreasing gradient in permafrost probability from 0.9 to 0.7 between the central part and the terminus of the western unit (Fig. 3).

2.1.2 Presenteseracae

Presenteseracae is a small (~ 600 m long and 300 m wide) debris-covered glacier located between ~ 4080 and 3800 m a.s.l., in a narrow, SW-facing cirque, ~ 300 m above and only 500 m east of Navarro (Fig. 3). The main presumed flow direction points towards 225° N. This landform has been thoroughly analysed by Monnier and Kinnard (2015). The debris-covered glacier exhibits rock glacier features in its lower part (Figs. 3, 4, and 7). The transverse and curved ridges (< 1.5 m high) and well-defined steep front (~ 10 m high) have appeared during the last 15 years. The permafrost model of Monnier and Kinnard (2015) gave a permafrost probability of 1 for the whole Presenteseracae landform. The authors also correlated the development of the cohesive flow-evocative rock glacier morphology with the low estimated sub-debris ice ablation rates, and demonstrated that the sediment store on Presenteseracae and the potential formation times are in agreement with common rock wall retreat rates. They concluded that Presenteseracae is a debris-covered glacier currently evolving into a rock glacier. In the upper part of the landform, the debris cover is very thin (a few centimetres) and bare ice exposures are frequent. The debris cover thickens to more than 60 cm in the lower part, where the rock glacier morphology develops below a steeper sloping segment. Push moraine ridges (Benn and Evans, 2010) occur at the surface above 3780 m a.s.l. (Fig. 3). The lower part, which displays a rock glacier morphology, is clearly composed of two adjacent lobes, dividing away from a morainic crest overridden by the landform (Fig. 4). Depressed meandering furrows where buried ice is exposed are also present (Fig. 3). During hot summer days, the water flowing in the northernmost furrow sinks down a hole just before the front.

2.2 Las Tetas

Las Tetas is located in the Colorado Valley, which is the uppermost part of the Elqui River valley, in the Norte Chico region of Chile ($30^\circ 10' S$, $69^\circ 55' W$; Fig. 1). Elevations in the Colorado Valley range between ~ 3100 and 6255 m a.s.l. The landform is located on the south-facing side of Cerro Las Tetas (5296 m a.s.l.), less than 1 km south of Tapado Glacier

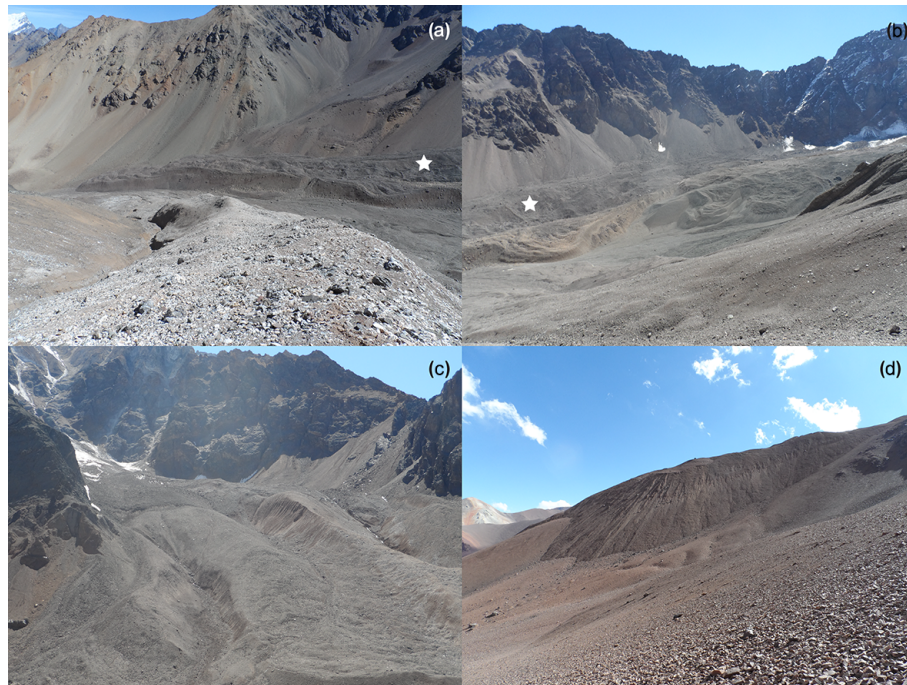


Figure 4. Photos of the lower (a) and upper part (b) of Navarro, seen from Presenteseracae; Presenteseracae seen from Navarro (c); and the terminal part of Las Tetas (d) seen from its northeastern surrounding area. The white stars on photos (a) and (b) indicate the main location of the central depression and related thermokarst morphology on Navarro (see Fig. 3).

(e.g. Ginot et al., 2006; Pourrier et al., 2014). The climate of the area is a semiarid mountain climate. At the La Laguna artificial dam (~ 3100 m a.s.l., 10 km west of the study site), the mean annual precipitation was 167 mm during the 1970–2009 period, and the MAAT was 8°C during the 1974–2011 period. The 0°C isotherm is located near 4000 m a.s.l. (Brenning, 2005; Ginot et al., 2006). Materials composing the rock basement belong to the Pastos Blancos Formation (Upper Palaeozoic; andesitic to rhyolitic volcanic rocks). A set of embedded latero-frontal moraines is encountered ~ 700 m downslope from the front of Las Tetas, between ~ 4170 and 4060 m a.s.l.

Las Tetas is a ~ 1 km long landform located between 4675 and 4365 m a.s.l. (Fig. 5). The main presumed flow direction points towards 140°N . The boundary between debris-covered and rock glacier morphology is clear, in the form of a large and deep furrow, and divides the landform in two approximately equal units. The upper unit is characterized by a chaotic and hummocky morphology, and vast (up to more than 50 m of diameter) and deep (up to 20 m) thermokarst depressions exposing bare ice generally along their south-facing walls. The lower part of the landform exhibits tension cracks superimposed onto the ridge-and-furrow pattern. The front of Las Tetas is prominent; including the talus slope at the bottom, which may bury sediments or outcrops downward, it is almost 100 m high (Figs. 4 and 5). According to the logistic regression-based empirical permafrost model proposed by Azócar (2013) for the area, the 0.75 probability

level crosses the landform in its central part (Fig. 5). Permafrost favourability index (PFI) values proposed by Azócar et al. (2016, 2017) are >0.7 in the upper part and between 0.6 and 0.7 in the lower part.

3 Material and methods

3.1 Satellite image and aerial photo processing

We acquired historical (prior to 2000) aerial photos and contemporary (after 2000) satellite images for the three study sites. Stereo pairs of aerial photos were inspected, selected, and scanned at the Geographic and Military Institute (IGM) of Chile. Scanning was configured in order to yield a ground resolution of 1 m. At Las Tetas, photos from 1978 and 2000 were selected; at Navarro and Presenteseracae, photos from 1955 and 2000 were selected. A stereo pair of Geoeye satellite images was also acquired for each site. The Geoeye imagery was acquired on 23 March 2012 and 14 February 2014 at Las Tetas and Navarro Valley, respectively, as panchromatic image stereo pairs (0.5 m of resolution) along with four bands in the near-infrared, red, green, and blue spectra (2 m of resolution).

Orthoimages, orthophotos, and altimetric information were generated from the data. The first step involved building a digital elevation model (DEM) from the stereo pair of Geoeye satellite images. The Geoeye images were triangulated using a rational polynomial camera (RPC) model sup-

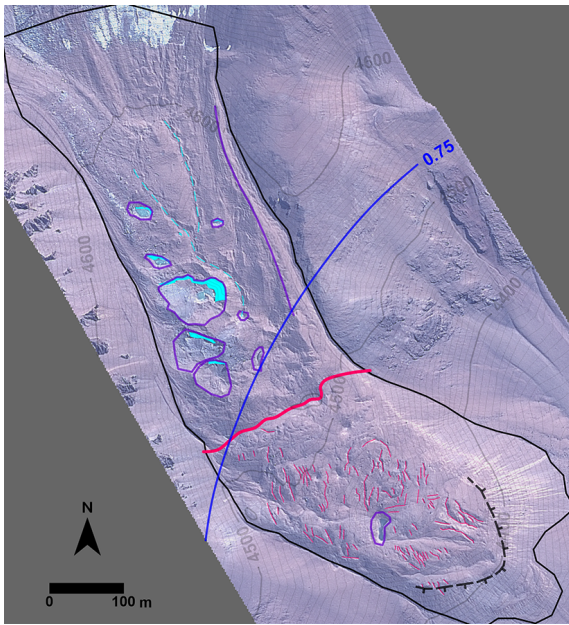


Figure 5. Map of the Las Tetas landform. See Fig. 2 for legend. The background of the map is the 2012 Geoeye image draped over the Geoeye DEM (see the “Material and methods” section).

plied by the data provider. The exterior orientation was constrained using one or two (according to the site) ground control points (GCPs) acquired with a differential GPS system in the field in 2014 over bedrock outcrops visible on the images. Sets of three-dimensional (3-D) points were extracted automatically using standard procedures of digital photogrammetry (Kääb, 2005) and edited manually to remove errors. A 2×2 m DEM was generated using triangular irregular network interpolation of the 3-D points. The same processing scheme was followed for the aerial photo stereo pairs using control points visible both on the Geoeye image and the aerial photo stereo pairs. The vertical bias of the aerial photo DEMs was calculated by comparison with the Geoeye DEMs over flat and stable areas outside the landform studied and was removed from the subsequent calculations (see below). The automatic and manual extraction of 3-D points from aerial photo stereo pairs proved to be challenging in steep areas with unfavourable viewing geometry. The process failed for the 1955 stereo pair of Navarro Valley, with only a very sparse set of 3-D points extracted and including possible errors, ruling out the possibility to generate a reliable and complete DEM and to estimate the vertical bias.

The Geoeye images were pan-sharpened and orthorectified using the Geoeye DEM. The aerial photos were then orthorectified using the corresponding DEMs, except when no reliable DEM could be obtained (as for 1955 at Navarro); in that case, the Geoeye DEM was used. The orthorectification was constrained by the internal camera information, tie points, and GCPs extracted during the process. The accuracy

Table 1. Errors generated during the aerial photo processing. The ground root mean square error (RMSE) relates to sets of ground control points (GCPs) extracted from the Geoeye orthoimage and used for the orthorectification of the aerial photos.

Site	Date	Horizontal ground RMSE (m)		Number of GCPs
		x	y	
Las Tetas	1978	1.13	1.16	10
	2000	0.33	0.54	8
Navarro Valley	1955	1.82	1.32	13
	2000	0.76	1.49	9

of the orthorectification was estimated using the GCPs. The root mean square error (RMSE) corresponding to the sets of GCPs at the different times is displayed in Table 1. The ground resolution of the orthophotos was then resampled at 0.5 m in order to equal that of the Geoeye products.

The altimetric information was used to calculate the elevation changes of the landforms between the different dates, after removal of the vertical bias. The total elevation change was further converted into annual rates of elevation change. As outlined by Lambiel and Delaloye (2004), elevation changes at the surface of rock glaciers may be explained by several and possibly concomitant factors: (i) downslope movement of the landform and advection of local topographic features, (ii) extensive or compressive flow, and (iii) melting or aggradation of internal ice. Therefore, it is difficult to unambiguously interpret elevation changes. Studying the Muragl rock glacier (Swiss Alps), Kääb and Vollmer (2000) highlighted how mass advection caused subtle elevation changes (between -0.20 and $+0.20$ m yr^{-1}), while surface lowering of up to -0.50 m yr^{-1} was considered as indicative of massive losses of ice. Accordingly, taking into account the range of values measured and the uncertainty (or detection threshold) on the measurements (see Table 2), we used an absolute value of 0.50 m yr^{-1} to generally discriminate between “moderate” and “large” vertical changes. The former were considered to relate primarily to the downslope expansion of the landform (including long profile adaptation and advection of topographic features) and, thus, to extensive flow; in the case of the latter, additional ice melting or material bulging by compression were considered necessary in the interpretation.

3.2 Image interpretation

The geomorphology of each landform was carefully interpreted from the orthoimages and orthophotos. First, we located and mapped the boundary between debris-covered and rock glacier morphology, according to the detailed criteria of differentiation presented in the Introduction. The thermokarst area was also monitored over time by mapping

Table 2. Uncertainty related to the measurement of annual elevation changes. Reported uncertainties correspond to 1 and 2-standard deviation (σ) probability of vertical errors for the generated DEMs. In Navarro Valley, no reliable DEM could be generated from the 1955 aerial photos, which explains the absence of data in the table for the 1955–2000 interval.

Site	Period	Vertical uncertainty (m yr^{-1})	
		1 σ (66 %)	2 σ (95 %)
Las Tetas	1978–2000	0.04	0.09
	2000–2012	0.22	0.43
Navarro Valley	1955–2000	–	–
	2000–2014	0.05	0.10

the thermokarst depressions at the surface of the landforms as polygonal shapes, and their total area was calculated. Salient and recently appeared features such as cohesive flow-convocative ridges on Presenteseracae and cracks on Las Tetas were also mapped.

3.3 Image feature tracking

We used image feature tracking in order to measure horizontal displacements at the surface of the landforms. Computer-programmed image feature tracking is a sub-pixel precision photogrammetric technique that has been widely used for studying the kinematics of glaciers, rock glaciers, and other mass movements. We followed the principles and guidelines provided by Käab and Vollmer (2000), Käab (2005), Wangenstein et al. (2006), Debella-Gilo and Käab (2011), and Heid and Käab (2012). We used ImGRAFT, which is an open-source image feature tracking toolbox for MATLAB (Messerli and Grinsted, 2015) using two orthoimages (from spaceborne, airborne, or terrestrial sensors) of the same area and resolution but at different times. All the orthoimages were pre-processed in order to enhance their contrast. Two template matching methods were tested: normalized cross-correlation (NCC) and orientation correlation (OC). The NCC method was found to yield more consistent results at the different sites and was thus used for this study. NCC gives an estimate of the similarity of image intensity values between matching entities in the orthoimage at time 1 (I_1) and their corresponding entities in the orthoimage at time 2 (I_2). In I_1 , a “search template” is defined around each pixel located manually or automatically inside a regular grid; the algorithm extracts this search template from I_1 and searches for it in I_2 within the area of a predefined search window (see, e.g., Fig. 2 in Debella-Gilo and Käab, 2011, p. 132); the algorithm then computes the NCC coefficient between the search template in I_1 and that in I_2 and moves the search template until the entire search window is covered. The location that yields the highest correlation coefficient within the search window is considered as the likely best match for the original location in I_1 . The sizes of the search template

Table 3. Sizes of search template and search window used for the image feature tracking.

Site	Period	Search template size (pixels)	Search window size (pixels)
Las Tetas	1978–2000	100	250
	2000–2012	150	250
Navarro	1955–2000	300	550
	2000–2014	50	100
Presenteseracae	1955–2000	150	400
	2000–2014	80	180

and search window were first defined based on image quality and the time period considered; larger template and search windows were used for long periods, as only larger-scale morphological features were expected to be preserved over periods of several decades. The final choice of template and search window size was then set after several iterations of the algorithm (see Table 3). The NCC algorithm was performed over the whole area of the landforms using a 10 m spacing grid. Snow-covered areas were delineated on each image and excluded from the analysis, leaving an additional buffer of 10 m around the snow masks.

Results from feature tracking generally need to be filtered, especially when dealing with old orthophotos (Wangenstein et al., 2006). In this study, the following filtering procedure was followed. (1) We excluded displacements smaller than the orthorectification error (RMSE, Table 1). (2) We excluded displacements exhibiting a signal-to-noise ratio (SNR) < 2 (as recommended by Messerli and Grinsted, 2015); SNR is the ratio between the maximum NCC coefficient and the average of the NCC coefficient’s absolute values in the search window, and can be used as an indicator of the “noise” in the results. (3) A directional filter was applied in order to eliminate vectors diverging excessively from one another, based on Heid and Käab (2012). For that purpose, the mean displacements in the X (\overline{du}) and Y (\overline{dv}) directions were calculated in a 5×5 m running window centred on each displacement vector. The displacement vector was excluded if its du and dv component exceeded \overline{du} and \overline{dv} , respectively, by more than 4 times the RMSE presented in Table 1. This last filtering step allowed excluding chaotic vectors with potential errors not removed by the first two filtering criteria, as well as highlighting areas with spatially coherent movement. Finally, the total displacements were converted to annual displacement rates and mapped.

Whereas all vectors obtained after filtering were mapped (see “Results and interpretations” and related figures), the final displacement statistics were calculated after removing upslope-pointing vectors (vectors deviating from more than $\pm 45^\circ$ from the landform longitudinal axis) (Table 4). These may include some remaining errors, but may also result from thermokarst degradation on debris-covered ice, as discussed later. As displacements statistics aimed at quantifying mean

Table 4. Summary statistics of horizontal displacements detected on the landform surfaces (see text for further details). The mean displacement (\bar{d} , m yr^{-1}) and standard deviation (σ , m yr^{-1}) are presented for the entire (snow-free) areas where movement was detected, and then only for the overlapping areas where movement was detected during both periods compared. The latter aimed at removing the spatial sampling bias when comparing movement statistics over time. n refers to the numbers of vectors retained and f to the corresponding fraction (%) of snow-free areas where movement was detected.

Site and period	Whole areas				Overlapping areas only		
	\bar{d}	σ	n	f	\bar{d}	σ	n
Navarro							
1955–2000	0.52	0.30	832	33	0.54	0.34	372
2000–2014	0.52	0.20	970	38	0.51	0.18	310
Presenteseracae							
1955–2000	1.04	0.46	219	15	1.10	0.41	73
2000–2014	0.96	0.47	162	12	0.82	0.40	63
Las Tetas							
1978–2000	0.88	0.35	79	15	0.69	0.21	18
2000–2012	0.86	0.45	163	31	0.65	0.37	30

downslope movement rates, these vectors were hence excluded from the calculation. Furthermore, for each landform, the mean annual displacement rate was re-calculated only over areas where movement was detected both during the historical (1955–2000 for Navarro Valley and 1978–2000 for Las Tetas) and recent (after 2000) periods in order to remove the spatial sampling bias (see Table 4). For this purpose, all the points present in a 20 m radius of each other's from one period to another were retained to estimate a mean displacement rate over a common area.

4 Results and interpretations

4.1 General performance of and insights provided by the methods

The methods used in this study first allowed to obtain series of images depicting at first sight conspicuous landscape evolutions: Figs. 6, 7, and 8 show the orthophotos and orthoimages obtained at each site together with the delineated boundary between debris-covered and rock glacier morphology areas and the front slope base at each time. These figures highlight how the landforms' landscape has changed over both historical (before 2000) and contemporary (after 2000) periods. Thermokarst areas could be easily mapped and calculated, except in 2000 at Las Tetas.

Reliable DEMs and related maps of elevation changes were obtained for the 2000–2014 period at Navarro (Fig. 10) and Presenteseracae (Fig. 12), and for both the 1978–2000 and 2000–2012 periods at Las Tetas (Figs. 13 and 14, re-

spectively). However, and as mentioned in the “Material and methods” section, no reliable and complete DEM could be obtained for the Navarro Valley in 1955, which explained the lack of elevation change measurements at Navarro and Presenteseracae.

The efficiency of the image feature tracking method varied according to the sites and periods but, on the whole, provided valuable information (Figs. 9–14 and Table 4). Filtering led to keeping between 12 and 38 % of the measured horizontal displacements according to the site and period (Table 4). The order of magnitude of the mean horizontal displacements is $0.50\text{--}1\text{ m yr}^{-1}$. Horizontal displacements were consistently detected in rock glacier areas, and much less in debris-covered glacier areas; Figs. 9–14 highlight spatially coherent flow vector patterns in the former, while the latter are characterized by a lack of movement detection and/or spatially chaotic patterns. This is consistent with the fact that the surface morphology of rock glaciers is more stable and preserved for longer times than the one of debris-covered glaciers, which is rather unstable and disrupt rapidly. Upslope-pointing vectors were kept in the figures in order to show that they frequently occur in sectors with thermokarst morphology where mass wasting processes are likely to occur. Finally, one will note that the most graphically striking results are obtained over the largest landform, i.e. Navarro (Figs. 9 and 10).

The interpretation of the main geomorphological evolution, elevation changes, and horizontal displacement patterns is summarized for each individual landform in Table 5a, b, and c, respectively, and the results are discussed jointly in the following section.

5 Discussion

The three cases studied have distinct significance in terms of glacier–rock glacier relationships and cryosphere persistence under ongoing climate change. Our results lead us to consider the following issues: (i) initial development of the landforms, (ii) differences between debris-covered and rock glacier areas, and (iii) current and future evolution of the landforms.

5.1 Initial landform development

Navarro and Las Tetas are composite landforms with a debris-covered glacier in their upper part and a rock glacier in their lower part. Considering the clear spatial organizations of surface features and the strong morphological boundaries, in particular the way the debris-covered glacier embeds into the rock glacier in the Navarro's western unit (Fig. 3) and the abrupt transition at Las Tetas (Fig. 5), these landforms most probably result from the (re)advance(s) of glaciers onto or in the back of pre-existing rock glaciers. Many other examples of such development of glacier–rock glacier assemblages have been studied and reported in the literature (Lugon et al., 2004; Haerberli, 2005; Käab and Kneisel, 2006;

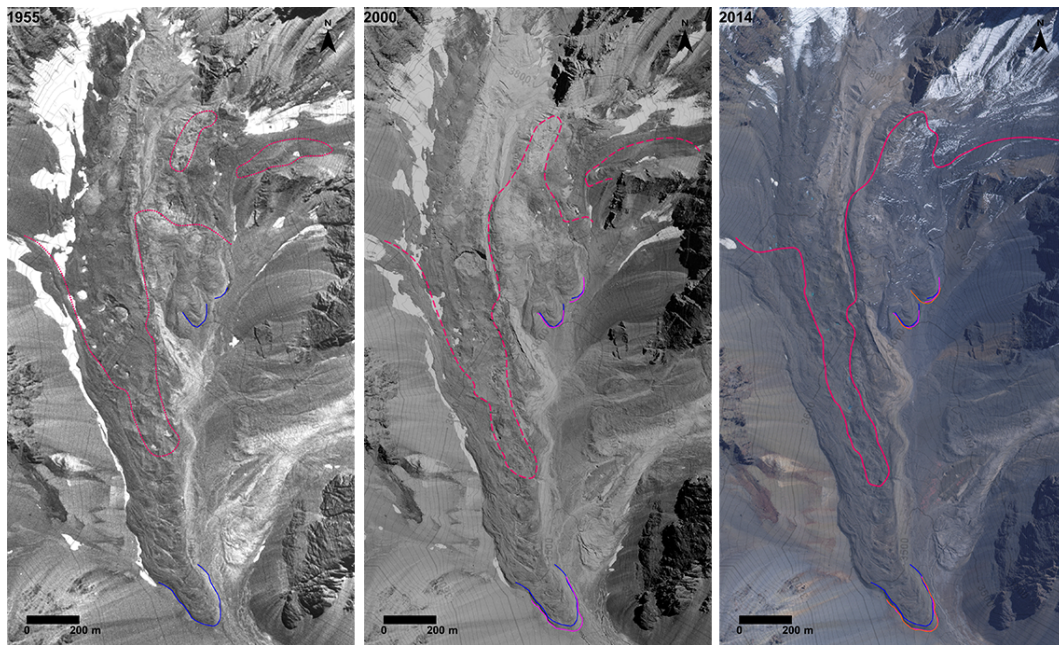


Figure 6. Sequence of orthophotos obtained for Navarro. The base of the landform front that could be reliably identified is indicated in colour (blue, magenta, and orange line in 1955, 2000, and 2014, respectively). At each date the boundary between debris-covered and rock glacier morphology is depicted with a red line (dotted in 1955, dashed in 2000, continuous in 2014).

Ribolini et al., 2007, 2010; Bodin et al., 2010; Monnier et al., 2011, 2014; Dusik et al., 2015). In the central part of the Navarro’s western unit, the elevated lateral margins exhibit cohesive flow-evocative ridges, which probably resulted from the lateral compression exerted by the glacier during its advance (“composite ridges” of the glaciological terminology; Benn and Evans, 2010, p. 492). Also, the boundary between the debris-covered and rock glacier morphologies in 1955 (Fig. 6) gives a minimum indication of the lowest advance of the debris-covered glaciers onto the rock glaciers. However, the origin and age of the rock glaciers located in the lower part of the landforms are almost impossible to assess. Nonetheless, considering the context, they may have developed following several glacier advances and moraine deposition phases, suggesting the idea of a cycle in the landform development (see section “Study sites” and the red circle in Fig. 3). Such a development has led to the rock glacier being cut off from the main rock debris sources (i.e. the rock walls up-valley), resulting in the rock glacier being dependent on the ability of the debris-covered glacier to provide material (debris and ice) required for the sustainment of the rock glacier.

Presenteseracae is a completely distinct case. As studied by Monnier and Kinnard (2015) and the present work, in 1955 Presenteseracae was a debris-covered glacier and is now a debris-covered glacier transforming into a rock glacier. The initial development phase or, in this case, the “glacier–rock glacier transformation” has been occurring over the last decades. In less than 20 years, the surface debris cover

spread over almost all of the northern part; a front appeared at the terminus, and cohesive-flow evocative ridges appeared in the lower part, perpendicular to flow vectors (Figs. 7, 11, and 12). The latter ridges may be related to emergent, debris-rich shear planes (Monnier and Kinnard, 2015) bent by the landform movement. Displacement speeds were high ($> 1 \text{ m yr}^{-1}$ on average) between 1955 and 2000, in agreement with the fast landscape evolution, before slowing down after 2000, which may reflect an acceleration of the transition towards a rock glacier. In the current state of our knowledge, what may have occurred in the internal structure in response to these drastic surface changes is uncertain: the continuous glacier core may, however, evolve into patches of buried ice progressively mixed with ice-mixed debris accumulated onto the surface.

5.2 Differences between debris-covered and rock glacier areas

Our study basically relied on the landscape differentiation between debris-covered and rock glacier areas. The criteria enounced and discussed in the Introduction section have been used to distinguish and partition the surface morphology of the landforms studied. Our subsequent results show that, at Navarro and Las Tetas, debris-covered and rock glacier areas are characterized by contrasting patterns of horizontal displacements and elevation changes. Flow patterns in rock glacier areas are conspicuous and spatially coherent and express the cohesive extensive flow of the landform in the di-

Table 5. (a) Summary of corresponding geomorphological evolution, elevation changes, horizontal displacements, and associated interpretations at Navarro for historical (1955–2000) and contemporary (2000–2014) periods. (b) Summary of corresponding geomorphological evolution, elevation changes, horizontal displacements, and associated interpretations at Presenteseracae for historical (1955–2000) and contemporary (2000–2014) periods. (c) Summary of corresponding geomorphological evolution, elevation changes, horizontal displacements, and associated interpretations at Las Tetras for historical (1978–2000) and contemporary (2000–2012) periods.

Geomorphological evolution	Elevation changes	Horizontal displacements	Interpretation
(a)			
Rock glacier morphology areas have expanded spatially between 1955 and 2014, both upward (eastern unit) and inward from the margin (western unit).	Elevation changes have been more pronounced and heterogeneous in debris-covered glacier morphology areas than in rock glacier morphology areas. In rock glacier areas, their moderate rates express the extensive flow of the landform (Fig. 10).	The area where movement was detected slightly increased (33 to 38%), during 1955–2000 and 2000–2014. The mean displacement speed decreased over snow-free, overlapping areas (Table 4).	The progression of the rock glacier morphology correlates with a decrease in thermokarst areas, an expansion of coherent flow patterns, and a general deceleration of the landform movement. This reflects the expansion of slow, coherent downslope creep with minimal surface disturbance (typical of rock glacier) as the main geomorphic process. In the central depression of the western unit, general downslope movement occurred along with ice-loss-related downwasting.
The upward progression of the rock glacier morphology areas has been particularly strong in the eastern unit, especially between 1955 and 2000.	Elevation changes have been moderate in the eastern unit (Fig. 10).	Figures 9 and 10 highlight conspicuously spatially coherent patterns of flow vectors in the eastern unit, especially between 1955 and 2000.	
In the western unit, the progression has been more limited and occurred inward from the margins, toward the central depression (Figs. 6, 9, and 10).	Very large surface lowering (until more than 1 m yr^{-1}) and moderate surface heaving alternate in the central depression (Fig. 10).	Many displacement spatially coherent vector patterns head towards the central depression (Figs. 9 and 10).	
Between 1955 and 2000, thermokarst area expanded from 11 950 to 16 520 m^2 , before shrinking by a factor of 2 in less than 15 years (8560 m^2 in 2014).	The most pronounced surface lowering occurs at thermokarst locations (Fig. 10).	At thermokarst locations, displacement vectors are grouped in poorly organized, chaotic patterns, frequently pointing upward (Figs. 9 and 10).	
(b)			
The geomorphological evolution at the surface has been very fast, with the apparition of a rock glacier morphology in the lower half of the landform since 2000, in agreement with the description and analysis given by Monnier and Kinnard (2015) (Figs. 7, 11, and 12).	Elevation changes have been spatially very heterogeneous for such a small-size landform between 2000 and 2014. Nevertheless, the major part of the surface exhibits moderate elevation changes, which is seen as the expression of the extensive flow of the landform (Fig. 12).	The area where movement was detected slightly decreased (15 to 12%) during 1955–2000 and 2000–2014, while the mean displacement speed decreased over snow-free, overlapping areas (Table 4). Horizontal flow vectors patterns are spatially more coherent in the lower than in the upper half of the landform (Figs. 11 and 12).	The geomorphological development, the distribution of flow vector patterns, and the deceleration of the landform movement point towards a transition towards rock glacier (Monnier and Kinnard, 2015); however, the decrease in the area where movement was detected does not corroborate such an interpretation. The absence of thermokarst at the surface of the landform for both periods studied may be explained by the small landform size, the cold conditions casted by the cirque topography (permafrost probability defined by the model in Fig. 3 is 1), the cirque floor slope, and/or even by the glacier–rock glacier transition phenomenon.
New morphological surface features, in the form of cohesive, flow-evocative downward (SE) convexly bent ridges, appeared in the lower-northern part of the landform (Figs. 3 and 7).	Elevation changes between 2000 and 2014 were generally moderate in the lower-northern part of the landform. Large surface heaving nevertheless occurred at the front of the landform (Fig. 12).	Horizontal displacement vectors in the lower part head towards SE (Figs. 11 and 12).	
No thermokarst.			

Table 5. Continued.

Geomorphological evolution	Elevation changes	Horizontal displacements	Interpretation
(c)			
The boundary between debris-covered and rock glacier morphology area has followed the overall displacement of the landform (Figs. 8, 13, and 14).	On the whole, elevation changes tended to decrease and be more spatially homogeneous from 1978 and 2000 to 2000 and 2012, with moderate rates expressing the extensive flow of the landform, especially in the lower rock glacier part (Figs. 13 and 14).	The area where movement was detected has strongly increased (15 to 31 %) between 1955 and 2000 as well as 2000 and 2014. The mean displacement speed decreased slightly (Table 4). However, between 2000 and 2012, the lower rock glacier part has displaced faster than the upper debris-covered glacier part (Fig. 14).	The decrease in thermokarst areas, the strong increase in movement detection areas, the apparition of coherent flow vectors patterns, and the deceleration of the whole landform support the idea that the rock glacier continues to develop. The higher displacement speed and the tension cracks in the lower rock glacier area nevertheless point towards an acceleration or even destabilization of the landform toward its terminus.
Tension cracks appeared in the lower part of the landform during the last decades (Figs. 5 and 8).		Whereas the mean displacement speed decreased slightly (Table 4), the lower part may be currently accelerating (Fig. 14).	
Thermokarst is striking by its aspect (depressions occur in the centre of coalescent mounds, reminiscent of impact craters) and its rapid evolution (Fig. 8). Between 1978 and 2012, thermokarst areas decreased 2-fold, from 23 248 m ² in 1978 to 11 099 m ² in 2012.	Large surface lowering occurred at the locations of thermokarst mounds and pounds, especially between 2000 and 2012 (Figs. 13 and 14).	Between 1978 and 2000, chaotic displacement patterns, with vectors frequently pointing upward, correlate with the thermokarst locations (Fig. 13). Between 2000 and 2012, very few vectors associated with thermokarst-related mass wasting are detected (Fig. 14).	

rection of the main longitudinal axis. Flow patterns in debris-covered glacier areas are either not detectable or, when detected, generally more chaotic. This low movement detection rate and chaotic organization of displacement patterns in debris-covered glacier areas can be explained by the inherently less cohesive mass flow and the unstable surface morphology resulting from the ablation of ice under a shallow debris layer. Elevation changes in debris-covered glacier areas have larger amplitudes and are spatially heterogeneous; in rock glacier areas, elevation changes are rather moderate and thus expressive of cohesive extensive flow. These different flow dynamics appear perfectly coherent with the definition of, and distinction made between, debris-covered and rock glaciers in the Introduction section.

5.3 Current evolution and its significance

5.3.1 Landscape evolution

All the landforms studied are characterized by a rapid landscape evolution over the last few decades. Changes occurred over the entire surface (Presenteseracae), in the contact/transition area between debris-covered and rock glaciers and in the debris-covered glacier area (Navarro), or even in both areas, though more subtly in the rock glacier area (Las

Tetas). This continuum in surface evolution perhaps best illustrates the process of glacial–periglacial transition. To our knowledge, an important result of our study not previously reported is the observed upward progression of the rock glacier areas which proceeds at the expense of the debris-covered glaciers on such composite landforms. At Presenteseracae, over a time span of a few decades, the rock glacier morphology has grown from being inexistent to covering approximately half the landform surface. At Navarro, rock glacier areas have subtly (in the western unit) or considerably (in the eastern unit) expanded, until, in the latter case, covering most parts of the essentially debris-covered glacier morphology present initially. As a first-order consideration, topoclimatic conditions seem to play a key role in this differentiated evolution: Presenteseracae and the eastern unit of Navarro are located in more shadowed and thus colder sites (see Figs. 3 and 5).

5.3.2 Dynamical evolution

The dynamical evolution correlates with the landscape evolution, to varying degrees according to the site. As stated in the Introduction, when areas with debris-covered glacier morphology evolve into areas with rock glacier morphology, changes occur in the surface energy balance and subsurface

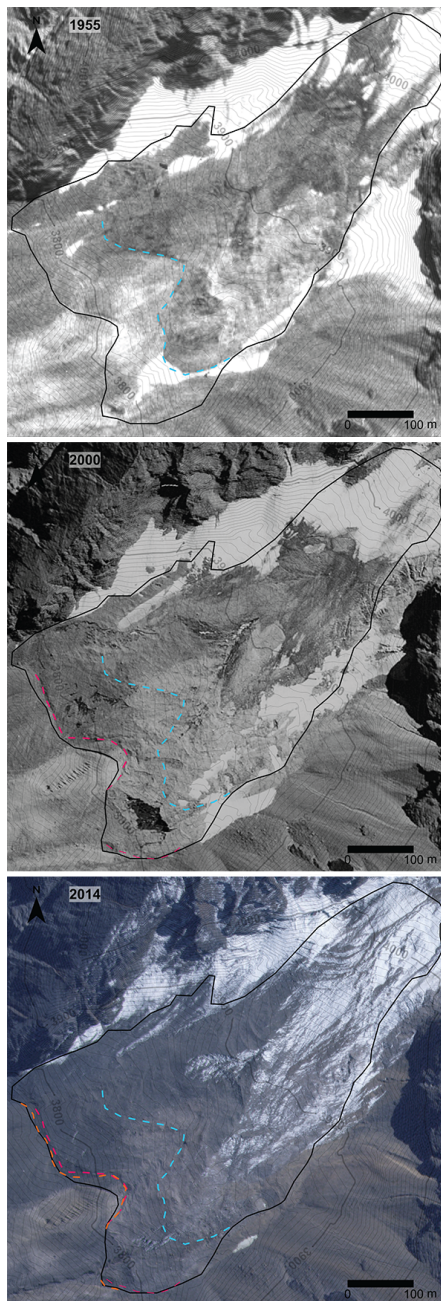


Figure 7. Sequence of orthophotos obtained for Presenteseracae. The base of the landform front that could be reliably identified is indicated in colour (blue, magenta, and orange line in 1955, 2000, and 2014, respectively). Note how the rock glacier morphology developed since 2000. In the southern part of the landform, it is nevertheless less well defined and more unstable; it is conspicuously cut by a central furrow and exhibits a few areas of bare ice over which debris slumps may occur. In the northern part of the landform, the rock glacier morphology is more developed; there is neither remaining bare ice area nor evidence of debris cover instability and sliding.

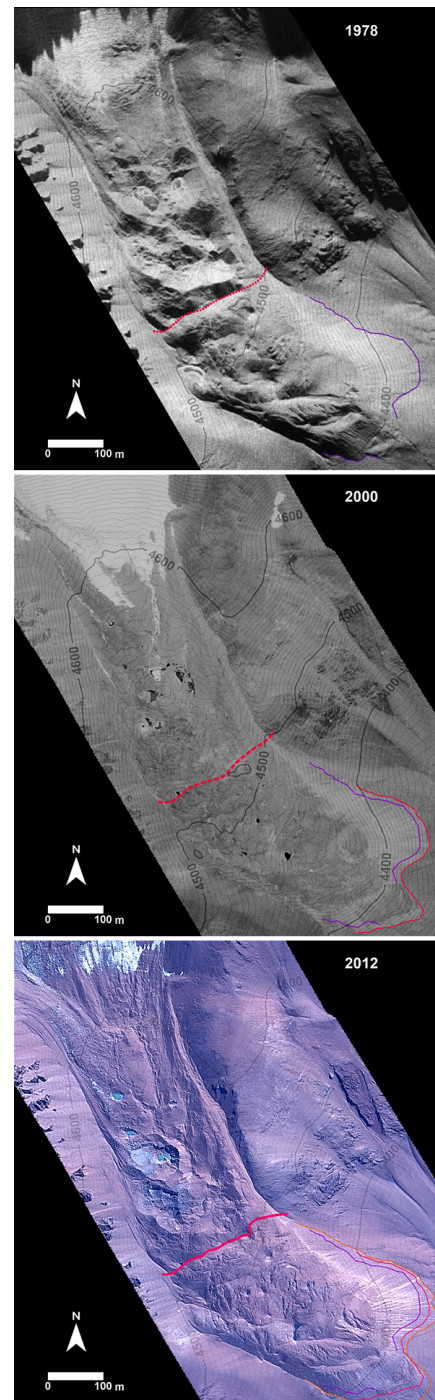


Figure 8. Sequence of orthophotos obtained for Las Tetas. The base of the landform front that could be reliably identified is indicated in colour (blue, magenta, and orange line in 1978, 2000, and 2012, respectively). At each date the boundary between debris-covered and rock glacier morphology is depicted with a red line (dotted in 1978, dashed in 2000, and continuous in 2012).

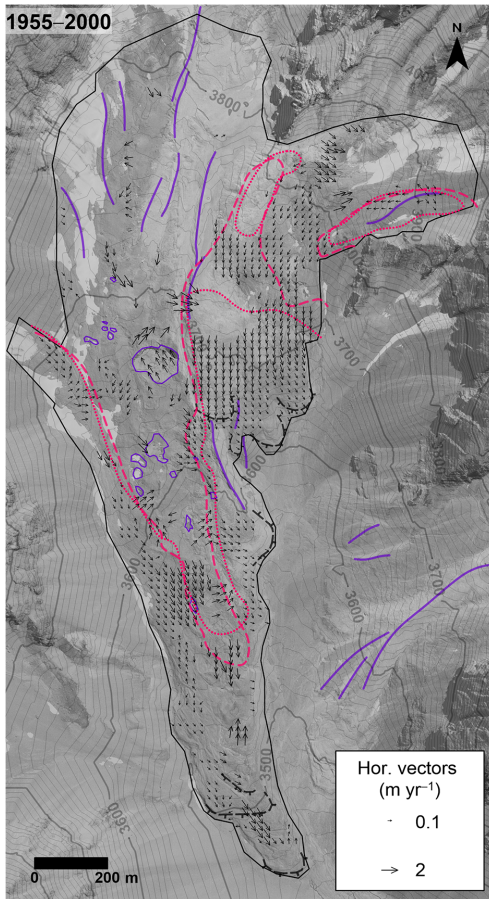


Figure 9. Horizontal displacements at the surface of Navarro between 1955 and 2000. The boundary between debris-covered and rock glacier morphology is depicted with a dotted red line in 1955 and with a dashed red line in 2014. Note that moraine crests and thermokarst depressions in 2000 are indicated. The background of the map is the 2000 orthophoto.

heat transfers, which is likely to result in changes in flow dynamics depending upon the topography and the topoclimatic context. The displacement speed of the three studied landforms has decreased over the study period, at least over the overlapping areas where movement was detected in the different periods (Tables 4, 5a, b, and c). Whereas in other areas of the world many studies have reported rock glaciers to be accelerating under the current climate warming trend (e.g. Roer et al., 2005, 2008; Delaloye et al., 2010; Kellerer-Pirklbauer and Kaufmann, 2012), the decreased velocity highlighted in this analysis suggests an increasing stabilization of the landforms as they evolved from debris-covered glacier bodies to rock glaciers. As the transition from debris-covered to rock glacier seems to be proceeding mainly from the terminus upward, the increasingly debris-rich, lower rock glaciers may exert an increasing buttressing force on the remaining debris-covered glacier upslope, causing a general deceleration of the landform.

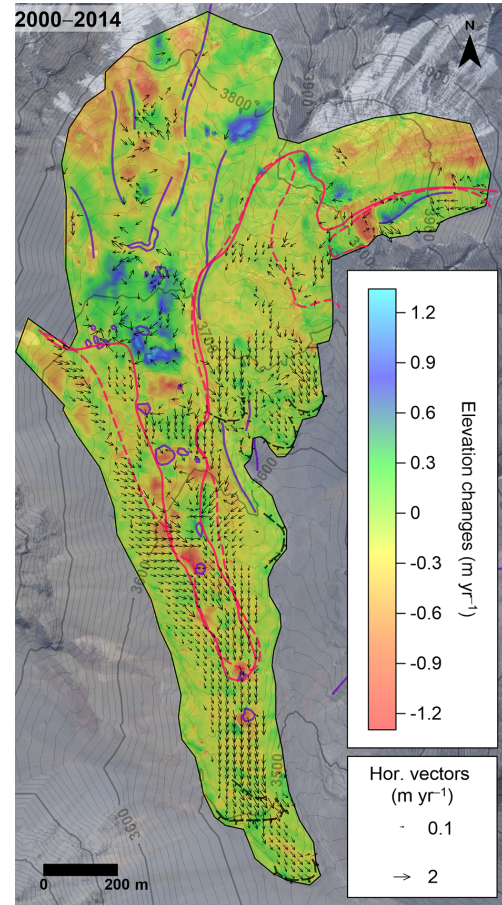


Figure 10. Horizontal displacements and elevation changes at the surface of Navarro between 2000 and 2014. The boundary between debris-covered and rock glacier morphology is depicted with a dashed red line in 2000 and with a continuous red line in 2014. Note that moraine crests and thermokarst depressions in 2014 are indicated. The background of the map is the 2014 Geoeye image.

At Las Tetas, however, increasing displacement speeds downslope and the apparition of tension cracks in the lower rock glacier area during the recent (2000–2012) period point towards a possible acceleration or even destabilization of the landform terminus (Figs. 3, 8, and 14). Such evolution may be related to the observed decrease in modelled permafrost probability along the landform area (Fig. 5) and the climate evolution in this region: Rabatel et al. (2011) reported a warming trend of $0.19\text{ °C decade}^{-1}$ for the 1958–2007 period in the Pascua-Lama area, 80 km north of Las Tetas, and Monnier et al. (2014) also reported a trend of $0.17\text{ °C decade}^{-1}$ for the 1974–2011 period in the Río Colorado area. Such evolution is reminiscent of reports of acceleration and destabilization phenomena over rock glaciers in response to air and permafrost temperature increases (e.g. Roer et al., 2005, 2008; Delaloye et al., 2010; Kellerer-Pirklbauer and Kaufmann, 2012).

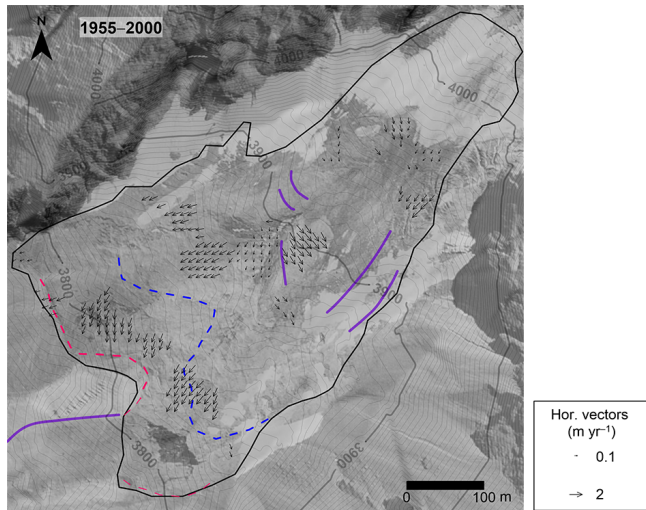


Figure 11. Horizontal displacements at the surface of Presenteseracae between 1955 and 2000. The position of the base of the front at the two dates is indicated with dashed lines, as in Fig. 7; push moraine ridges in the upper part are also indicated. The background of the map is the 2000 orthophoto.

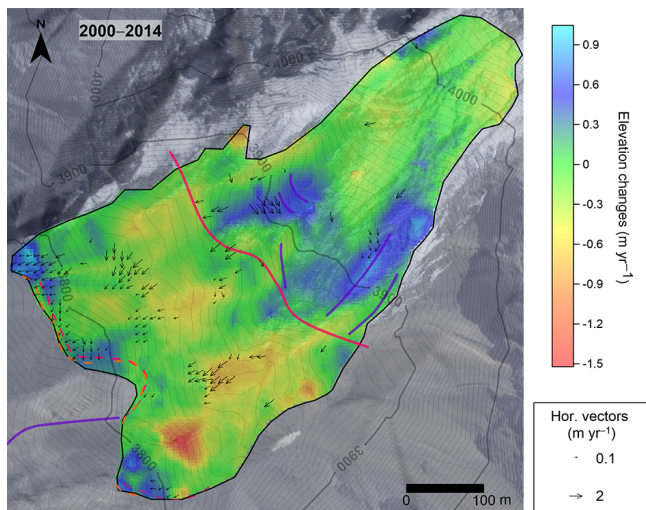


Figure 12. Horizontal displacements and elevation changes at the surface of Presenteseracae between 2000 and 2014. The position of the base of the front at the two dates is indicated with dashed lines, as in Fig. 7; the boundary between rock glacier and debris-covered glacier features and push moraine ridges in the upper part are indicated. The background of the map is the 2014 Geoye image.

5.3.3 Final diagnostics and future evolution of the landforms

According to the results and interpretations presented for the Navarro's eastern part and Presenteseracae, rock glaciers can develop at the expense of debris-covered glaciers, by an upward progression of their morphology and correlative widespread development of cohesive mass flow. These

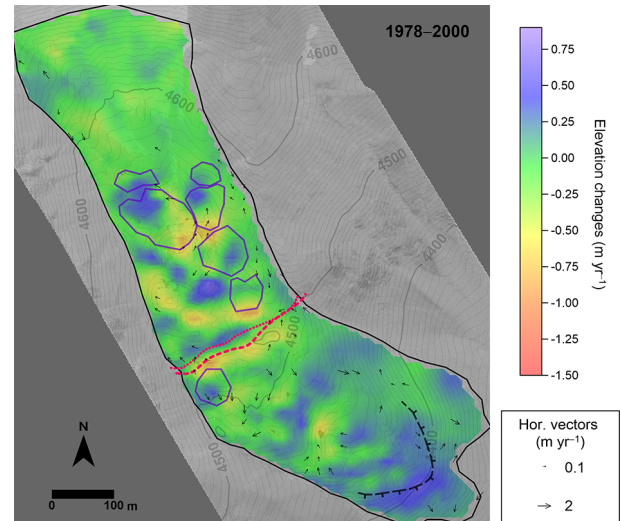


Figure 13. Horizontal displacements and elevation changes at the surface of Las Tetas between 1978 and 2000. The boundary between debris-covered and rock glacier morphology is depicted with a dotted red line in 1978 and with a dashed red line in 2000. Thermokarst depressions in 1978 are indicated. Thermokarst areas could not be accurately and reliably delineated on the 2000 orthophoto and are hence not mapped. The background of the map is the 2000 orthophoto.

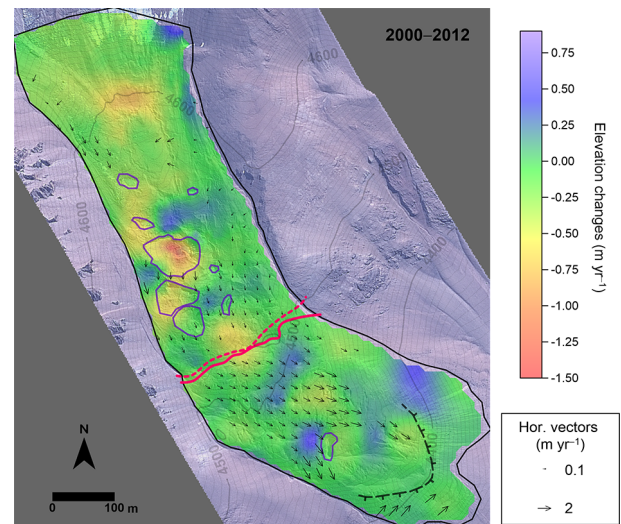


Figure 14. Horizontal displacements and altitudinal changes at the surface of Las Tetas between 2000 and 2012. The boundary between debris-covered and rock glacier morphology is depicted with a dashed red line in 2000 and with a continuous red line in 2012. Note that thermokarst depressions in 2012 are indicated. The background of the map is the 2012 Geoye image.

are true cases of debris-covered glaciers evolving in rock glaciers (see Introduction: type iii). At Presenteseracae, however, the flow does not appear as strikingly cohesive as for the Navarro's western unit, possibly due to the smaller size of the

landform as well as a steeper slope that may constitute a limiting dynamical parameter (Monnier and Kinnard, 2015). As these two landforms are located in favourable topoclimatic conditions, they should thus pursue their evolution towards rock glaciers. Despite the important insights presented by our study, it must be stressed that the evolution of the internal structure in response to morphological and dynamical changes at the surface remains unknown; it would require decades of borehole and geophysical survey monitoring to properly assess this. However, the transition may proceed by fragmentation of the glacier ice core and its mixing with debris and other types of ice (interstitial, intrusive) entrained from the surface. This is an alternative to the common and controverted model of the glacier ice-cored rock glacier where the evolution of the landform is controlled by the expansion and creep of a massive and continuous core of glacier ice (e.g. Potter, 1972; Whalley and Martin, 1992; Potter et al., 1998).

The Navarro's western unit and Las Tetas are more commonly known cases of assemblages that have formed and evolved in reaction to the superimposition/embedding of glaciers onto or in the back of rock glaciers and their subsequent dynamical interactions (see Introduction: type i). In both cases, the progression of the rock glacier at the expense of the debris-covered glacier is rather limited (Navarro's western unit) or null (Las Tetas). It is difficult to assert here whether the debris-covered glaciers are "pushing away" the rock glaciers or whether the latter are "pulling" the former; both processes probably occur (see also Sect. 5.3.2.). The dynamical links between both units certainly constitute a complex issue deserving more attention. Furthermore, as these whole landforms continue to advance, the rock glaciers could plausibly become entirely isolated from their main debris source in the upper cirques, while the increasingly warming conditions could cause the debris-covered glacier to become stagnant or disappear. Also, as the rock glaciers penetrate into areas with less favourable topoclimatic conditions, their future sustainment can be questioned.

6 Conclusion

We have used remote sensing techniques, including imagery orthorectification, DEM comparisons, and image feature tracking, in order to depict and measure the geomorphological evolution, elevation changes, and horizontal displacements of three glacier–rock glacier transitional landforms in the central Andes of Chile over a human-life timescale. Our study highlights how, as climate changes and mountain landscapes and their related dynamics shift, the glacial and periglacial realms can strongly interact. The pluri-decadal landscape evolution at the three studied sites is noticeable: rock glacier morphology areas expanded, as well as the movement detection area in image feature tracking; thermokarst reduced; elevation changes tended to become

more homogenous; and the mean horizontal displacement decreased and spatially coherent flow patterns enhanced. These overall results point toward the geomorphological and dynamical expansion of rock glaciers. However, the modalities and significance vary between sites. Navarro and Las Tetas are composite landforms resulting from the alternation between glacier (re)advance and rock glacier development phases; they currently exhibit an upward progression of the rock glacier morphology with associated cohesive mass flow and surface stabilization, or ice-loss-related downwasting and surface destabilization features. Presenteseracae is a special case of small debris-covered glacier that has evolved into a rock glacier during the last decades, with the rock glacier morphology having mostly developed ~15 years ago. Topoclimatic conditions appear to have been determinants in the landforms' evolution and, by extrapolation, could thus be expected to exert an important control on the development and conservation of underground ice in high-mountain catchments. From the latter point of view, our study stresses how spatial and dynamical interactions between glaciers and permafrost create composite landforms that may be more perennial than transitory: depending on the frequency of glacial–periglacial cycles, they participate in sustaining a hybrid cryospheric landscape that is potentially more resilient against climate change. This conclusion is of societal importance considering the location of the studied landforms in semiarid areas and the warming and drying climate predicted for the coming decades (Bradley et al., 2006; Fuenzalida et al., 2006).

We have furthermore provided new insights into the glacier–rock glacier transformation problem. Most of the common and previous glacier–rock glacier evolution models depicted a "continuum" process based on the preservation of an extensive core of buried glacier ice. However, our findings rather suggest that the transformation of a debris-covered glacier into a rock glacier may proceed from the upward progression of the rock glacier morphology at the expense of the debris-covered glacier, in association with an expanding cohesive mass flow regime and a probable fragmentation of the debris-covered glacier into an ice–rock mixture with distinct flow lobes. The highlighted importance of topoclimatic conditions and corresponding morphologic evolutions also supports the inclusion of the permafrost criterion within the rock glacier definition.

Data availability. Aerial data were acquired in the framework of a partnership with the private Juncal Natural Park. The latter has imposed restrictions on the publications of direct aerial views of the park. At the moment, access to the original data set is therefore not possible.

Competing interests. The authors declare that they have no conflict of interest.

Acknowledgements. This study is part of the Project Fondecyt Regular no. 1130566 entitled “Glacier–rock glacier transitions in shifting mountain landscapes: peculiar highlights from the central Andes of Chile”. Fondecyt is the National Fund for Research and Technology in Chile. The authors want to thank Arzhan Surazakov, who performed the image processing, and Valentin Brunat, who was involved in the software handling and related data management in the framework of a master’s thesis supported by the above-mentioned project. The authors also thank Andreas Kääh and Christophe Lambiel for their important help in improving this manuscript, as well as the associate editor for final edition and language corrections.

Edited by: Arjen Stroeven

Reviewed by: Christophe Lambiel and Andreas Kääh

References

- Azócar, G. F.: Modelling of permafrost distribution in the semiarid Chilean Andes, Master Thesis, University of Waterloo, Canada, 2013.
- Azócar, G. F. and Brenning, A.: Hydrological and geomorphological significance of rock glaciers in the dry Andes, Chile (27°–33° S), *Permafrost Periglac.*, 21, 42–53, 2010.
- Azócar, G. F., Brenning, A., and Bodin, X.: Permafrost Favourability Index Map for the Chilean semi-arid Andes, Online data visualization, available at: www.andespermafrost.com (last access: 21 April 2017), 2016.
- Azócar, G. F., Brenning, A., and Bodin, X.: Permafrost distribution modelling in the semi-arid Chilean Andes, *The Cryosphere*, 11, 877–890, <https://doi.org/10.5194/tc-11-877-2017>, 2017.
- Barsch, D.: Permafrost creep and rock glaciers, *Permafrost Periglac.*, 3, 175–188, 1992.
- Benn, D. I. and Evans, D. J. A.: *Glaciers and Glaciation*, Routledge, London, 2010.
- Berthling, I.: Beyond confusion: rock glaciers as cryo-conditioned landforms, *Geomorphology*, 131, 98–106, 2011.
- Bodin, X., Brenning, A., Rojas, F.: Status and evolution of the cryosphere in the Andes of Santiago (Chile, 33.5° S), *Geomorphology*, 118, 453–464, 2010.
- Bosson, J.-B. and Lambiel, C.: Internal structure and current evolution of very small debris-covered glacier systems located in alpine permafrost environments, *Front. Earth Sci.*, 4, 1–17, 2016.
- Bown, F., Rivera, A., and Acuña, C.: Recent glacier variations at the Aconcagua basin, central Chilean Andes, *Ann. Glaciol.*, 48, 43–48, 2008.
- Bradley, R. S., Vuille, M., Diaz, H. F., and Vergara, W.: Threats to water supply in the tropical Andes, *Science*, 23, 1755–1756, 2006.
- Brenning, A.: Climatic and geomorphological controls of rock glaciers in the Andes of central Chile: combining statistical modelling and field mapping, PhD Thesis, Humboldt University, Berlin, 2005.
- Cogley, J. G., Hock, R., Rasmussen, L. A., Arendt, A. A., Bauder, A., Braithwaite, P., Jansson, P., Kaser, G., Möller, M., Nicholson, L., and Zemp, M.: Glossary of Glacier Mass Balance and Related Terms, UNESCO-IHP, Paris, 2011.
- Debella-Gilo, M. and Kääh, A.: Sub-pixel precision image matching for measuring surface displacements on mass movements using normalized cross-correlation, *Remote Sens. Environ.*, 115, 130–142, 2011.
- Degenhardt, J. J.: Development of tongue-shaped and multilobate rock glaciers in alpine environments – Interpretations from ground penetrating radar surveys, *Geomorphology*, 109, 94–107, 2009.
- Delaloye, R., Lambiel, C., and Gärtner-Roer, I.: Overview of rock glacier kinematics research in the Swiss Alps, *Geogr. Helv.*, 65, 135–145, <https://doi.org/10.5194/gh-65-135-2010>, 2010.
- Dusik, J.-M., Leopold, M., Heckmann, T., Haas, F., Hilger, L., Morche, D., Neugirg, F., and Becht, M.: Influence of glacier advance on the development of the multipart Riffeltal rock glacier, Central Austrian Alps, *Earth Surf. Proc. Land.*, 40, 965–980, 2015.
- Fuenzalida, H., Aceituno, P., Falvey, M., Garreaud, R., Rojas, M., and Sánchez, R.: Estudio de la variabilidad climática en Chile para el siglo XXI, Departamento de Geociencias, Universidad de Chile, Santiago, 2006.
- Ginot, P., Kull, C., Schotterer, U., Schwikowski, M., and Gäggeler, H. W.: Glacier mass balance reconstruction by sublimation induced enrichment of chemical species on Cerro Tapado (Chilean Andes), *Clim. Past*, 2, 21–30, <https://doi.org/10.5194/cp-2-21-2006>, 2006.
- Haerberli, W.: Creep of mountain permafrost: internal structure and flow of alpine rock glaciers, *Mitteilungen der Versuchsanstalt für Wasserbau, Hydrologie und Glaziologie*, Nr. 77, Zürich, 1985.
- Haerberli, W.: Investigating glacier–permafrost relationships in high-mountain areas: historical background, selected examples and research needs, in: *Cryospheric systems: glaciers and permafrost*, edited by: Harris, C. and Harris, J. B., The Geological Society, London, 29–38, 2005.
- Haerberli, W., Hallet, B., Arenson, L., Elconin, R., Humlum, O., Kääh, A., Kauffmann, V., Ladanyi, B., Matsuoka, M., Springman, S., and Vonder Mühl, D.: Permafrost creep and rock glacier dynamics, *Permafrost Periglac.*, 17, 189–214, 2006.
- Heid, T. and Kääh, A.: Evaluation of existing image matching methods for deriving glacier surface displacements globally from optical satellite imagery, *Remote Sens. Environ.*, 118, 339–355, 2012.
- Humlum, O.: The geomorphic significance of rock glaciers: estimates of rock glacier debris volumes and headwall recession rates in West Greenland, *Geomorphology*, 35, 41–67, 2000.
- Janke, J. R., Bellisario, A. C., and Ferrando, F. A.: Classification of debris-covered glaciers and rock glaciers in the Andes of central Chile, *Geomorphology*, 241, 98–121, 2015.
- Johnson, P. G.: Glacier–rock glacier transition in the Southwest Yukon territory, Canada, *Arctic Alpine Res.*, 12, 195–204, 1980.
- Kääh, A.: Remote sensing of mountain glaciers and permafrost, Zürich University, Switzerland, 2005.
- Kääh, A., Haerberli, W., and Gudmundsson, G. H.: Analysing the creep of mountain permafrost using high precision aerial photogrammetry: 25 years of monitoring Gruben rock glacier, Swiss Alps, *Permafrost Periglac.*, 8, 409–426, 1997.
- Kääh, A. and Kneisel, C.: Permafrost creep within a recently deglaciated forefield: Muragl, Swiss Alps, *Permafrost Periglac.*, 17, 79–85, 2006.
- Kääh, A. and Vollmer, M.: Surface geometry, thickness changes and flow fields on creeping mountain permafrost: Automatic extrac-

- tion by digital image analysis, *Permafrost Periglac.*, 11, 315–326, 2000.
- Kääb, A. and Weber, M.: Development of transverse ridges on rock glaciers: field measurements and laboratory experiments, *Permafrost Periglac.*, 15, 379–391, 2004.
- Kellerer-Pirklbauer, A. and Kaufmann, V.: About the relationships between rock glacier velocity and climate parameters in Central Austria, *Austrian Journal of Earth Sciences*, 105, 94–112, 2012.
- Krainer, K. and Mostler, W.: Reichenkar rock glacier: a glacier-derived debris-ice system in the western Stubai Alps, Austria, *Permafrost Periglac.*, 11, 267–275, 2000.
- Lambiel, C. and Delaloye, R.: Contribution of real-time kinematic GPS in the study of creeping mountain permafrost: examples from the Western Swiss Alps, *Permafrost Periglac.*, 15, 229–241, 2004.
- Lugon, R., Delaloye, R., Serrano, E., Reynard, E., Lambiel, C., and González-Trueba, J. J.: Permafrost and Little Ice Age glacier relationships, Posets Massif, Central Pyrenees, Spain, *Permafrost Periglac.*, 15, 207–220, 2004.
- Messerli, A. and Grinsted, A.: Image Georectification and feature tracking toolbox: ImGRAFT, *Geoscientific Instrumentation, Methods and Data Systems*, 4, 23–34, 2015.
- Monnier, S. and Kinnard, C.: Reconsidering the glacier to rock glacier transformation problem: new insights from the central Andes of Chile, *Geomorphology*, 238, 47–55, 2015.
- Monnier, S., Kinnard, C., Surazakov, A., and Bossy, W.: Geomorphology, internal structure, and successive development of a glacier foreland in the semiarid Andes (Cerro Tapado, upper Elqui Valley, 30°08' S, 69°55' W), *Geomorphology*, 207, 126–140, 2014.
- Monnier, S., Camerlynck, C., Rejiba, F., Kinnard, C., Feuillet, T., and Dhemaied A.: Structure and genesis of the Thabor rock glacier (Northern French Alps) determined from morphological and ground-penetrating radar survey, *Geomorphology*, 134, 269–279, 2011.
- Nakawo, M., Raymond, C. F., and Fountain, A. (Eds.): *Debris-covered Glaciers*, IAHS Press, Wallingford, 2000.
- Potter, N.: Ice-cored rock glacier, Galena Creek, Northern Absaroka Mountains, Wyoming, *Geol. Soc. Am. Bull.*, 83, 3025–3058, 1972.
- Potter, N., Steig, E. J., Clark, D. H., Speece, M. A., Clark, G. M., and Updike, A. U.: Galena Creek rock glacier revisited – new observations on an old controversy, *Geogr. Ann. A*, 80, 251–265, 1998.
- Pourrier, J., H., Kinnard, C., Gascoïn, S., and Monnier, S.: Glacier meltwater flow paths and storage in a geomorphologically complex glacial foreland: the case of the Tapado glacier, dry Andes of Chile (30° S), *J. Hydrol.*, 519, 1068–1083, 2014.
- Rabatel, A., Castebrunet, H., Favier, V., Nicholson, L., and Kinnard, C.: Glacier changes in the Pascua-Lama region, Chilean Andes (29° S): recent mass balance and 50 yr surface area variations, *The Cryosphere*, 5, 1029–1041, <https://doi.org/10.5194/tc-5-1029-2011>, 2011.
- Ragettli, S., Cortés, G., McPhee, J., and Pellicciotti, F.: An evaluation of approaches for modelling hydrological processes in high-elevation, glacierized Andean watersheds, *Hydrol. Process.*, 28, 5774–5695, 2012.
- Rangecroft, S., Harrison, S., Anderson, K., Magrath, J., Castel, A. P., and Pacheco, P.: Climate change and water resources in arid mountains: an example from the Bolivian Andes, *Ambio*, 42, 852–863, 2013.
- Ribolini, A., Chelli, A., Guglielmin, M., and Pappalardo, M.: Relationships between glacier and rock glacier in the Maritime Alps, Schiantala valley, Italy, *Quaternary Res.*, 68, 353–363, 2007.
- Ribolini, A., Guglielmin, M., Fabre, D., and Schoeneich, P.: The internal structure of rock glaciers and recently deglaciated slopes as revealed by geoelectrical tomography: insights on permafrost and recent glacial evolution in the Central and Western Alps (Italy–France), *Quaternary Sci. Rev.*, 29, 507–521, 2010.
- Roer, I., Kääb, A., and Dikau, R.: Rockglacier acceleration in the Turtmann valley (Swiss Alps): probable controls, *Norsk Geografisk Tidsskrift (Norwegian Journal of Geography)*, 59, 157–163, 2005.
- Roer, I., Haeberli, W., Avian, M., Kaufmann, V., Delaloye, R., Lambiel, C., and Kääb, A.: Observations and considerations on destabilizing active rockglaciers in the European Alps, in: *Proceedings of the Ninth International Conference on Permafrost*, edited by: Kane, D. L. and Hinkel, K. M., University of Alaska, Fairbanks, 1505–1510, 2008.
- Schroder, J. F., Bishop, M. P., Copland, L., and Sloan, V. F.: Debris-covered glaciers and rock glaciers in the Nanga Parbat Himalaya, Pakistan, *Geogr. Ann. A*, 82, 17–31, 2000.
- Seppi, R., Zanozer, T., Carton, A., Bondesan, A., Francese, R., Carturan, L., Zumiani, M., Giorgi, M., and Ninfo, A.: Current transition from glacial to periglacial processes in the Dolomites (South-Eastern Alps), *Geomorphology*, 228, 71–86, 2015.
- Wangensteen, B., Guðmundsson, A., Kääb, A., Farbrót, H., and Etzel-müller, B.: Surface displacements and surface age estimates for creeping slope landforms in Northern and Eastern Iceland using digital photogrammetry, *Geomorphology*, 80, 59–79, 2006.
- Whalley, W. B. and Martin, H. E.: Rock glaciers. II. Models and mechanisms, *Prog. Phys. Geog.*, 16, 127–186, 1992.